Arch. Mech., 40, 5–6, pp. 725–740, Warszawa 1988

Statistical approach to elastoplastic behaviour of polycrystals at finite deformations

P. LIPINSKI, M. BERVEILLER and F. CORVASCE (METZ)

THE AIM of this study is to determine the elastoplastic properties of metallic polycrystals at large strains using the statistical methods developed by Kröner. The large number of microfields describing the internal structure evolution is taken into account. The evolution laws for these parameters are recalled or proposed. A few numerical results are finally presented which illustrate the evolution of the internal structure. Special attention is focussed on internal stresses and on stored energy linked with these second-order residual stresses and their influence on the overall behaviour of the polycrystal.

Celem pracy jest określenie sprężysto-plastycznych własności polikryształów metalicznych w zakresie dużych deformacji przy użyciu metod statycznych rozwiniętych przez Krönera. Rozważono wiele mikropól opisujących ewolucję struktury wewnętrznej. Dla parametrów charakteryzujących te pola zaproponowano nowe (lub wykorzystano znane) równania ewolucji. Przedstawiono kilka przykładów numerycznych, które ilustrują ewolucję struktury wewnętrznej. Ze szczególną uwagą przeanalizowano problem wewnętrznych naprężeń resztkowych oraz energii ukrytej związanej z tymi naprężeniami, pod kątem ich wpływu na globalne zachowanie się polikryształu.

Целью работы является определение упруго-пластических свойств металлических поликристаллов в области больших деформаций при использовании статистических методов развитых Кренером. Рассмотрено много микрополей, описывающих эволюцию внутренней структуры. Для параметров, характеризующих эти поля, предложены новые или использованы известные уравнения эволюции. Представлено несколько численных примеров, которые иллюстрируют эволюцию внутренней структуры. С особенным вниманием проанализирована проблема внутренних остаточных напряжений и внутренней энергии, связанной с этими напряжениями под углом их влияния на глобальное поведение поликристалла.

List of notations

- $\mathbf{B}(x)$ concentration tensor,
- $\mathbf{C}$ elasticity tensor,
- $\mathbf{d}$ local strain rate tensor,
- $\mathbf{D}$ overall strain rate tensor,
- $\mathbf{g}(x)$ local velocity gradient,
- $\mathbf{g}^0(x)$ velocity gradient of some fictitious reference medium,
- $\mathbf{G}$ overall velocity gradient,
- $\mathscr{G}$ Green tensor for the fictitious medium,
- H^{gh} hardening matrix,
- $\mathbf{I}$ identity tensor,
- l local elastoplastic tangent moduli tensor,
- δl deviation part of l,
- $\mathbf{L}^0$ tangent moduli tensor of some fictitious and homogeneous medium,
- $\mathbf{L}^{\mathrm{eff}}$ effective elastoplastic tangent moduli tensor,
- $\dot{\mathbf{n}}$ local nominal stress rate tensor,
- $\dot{\mathbf{N}}$ overall nominal stress rate tensor,

$\mathbf{m}^h \otimes \mathbf{n}^h$ orientation tensor of the h-th slip system,
$\mathbf{R}^h$ symmetric part of the orientation tensor,
$\mathbf{Q}^h$ antisymmetric part of the orientation tensor,
S_t current external surface of the solid,
V_t current volume of the solid,
$\mathbf{w}$ local spin tensor,
$\mathbf{W}$ overall spin tensor,
$\dot{\gamma}^h$ plastic slip rate on the h-th system,
τ_c critical shear stress,
$\boldsymbol{\sigma}$ Cauchy stress tensor,
$\overset{\nabla}{\boldsymbol{\sigma}}{}^*$ Jaumann-Zaremba true stress rate with respect to the crystal lattice.

1. Introduction

AS FAR as linear elastic properties of the metallic polycrystal are concerned, a complete solution to the averaging problem may be obtained via the recently developed systematic statistical theories [1, 2, 3]. Until very recently, studies on plastic or elastoplastic properties of inhomogeneous materials have been limited to the applications of SACHS [4] and TAYLOR [5] models or eventually to the different extensions of these.

It is obvious that the processes of metal forming lead, in general, to the finite elastoplastic strains which simultaneously modify the internal structure and mechanical state of the deformed material. The internal structure is essentially concerned with the critical shear stress on all glide systems of the polycrystal, the second-order internal stresses associated with plastic incompatibilities between grains and the crystallographic and morphological textures. In order to describe well the deformation process, and especially complex loading histories, the evolution rules for these micro-parameters must be established and taken into consideration. The first real tentatives of microstructure evolution modelling are related with the application of the self-consistent method to the elastoplasticity of metallic polycrystals [6, 7, 8, 9]. Parallelly the elastoviscoplastic or viscoplastic models were developed [10, 11].

The aim of this study is to answer the question of how to incorporate the evoked micro-parameters into the polycrystal modelling and to give the rational evolution laws for them. To start with, we recall very briefly the theoretical bases of the self-consistent method at finite deformations. In the second section the single crystal behavior is reviewed. Special attention is paid to the evolution rule of the critical shear stresses on slip systems.

Finally, a few illustrative examples are presented for a FCC polycrystal modelled by a set of 100 grains (inclusions) with isotropic elasticity. The evolution laws for the crystallographic and morphological textures and internal stresses are proposed and discussed with respect to the obtained results.

2. Integral equations and its resolution methods

As it was demonstrated in [9], the self-consistent method is in fact only a particular case of the more general concentration problem whose aim is to connect local and overall mechanical measures such as nominal stress rate $\dot{\mathbf{n}}$ and velocity gradient g. IWAKUMA

and NEMAT-NASSER [12] proposed the self-consistent model at finite strain based on the general self-consistent scheme developed by HILL [13]. They applied this model to the case of plane polycrystal idealization by imposing only two active slip systems by grain. In this study we use the results obtained in [9].

Let us suppose, for the moment, that single crystal behavior may be characterized by the relation

$$\dot{n}_{ij} = l_{ijkl} g_{lk}. \tag{2.1}$$

Thus the considered problem may be described by the following set of equations:

equilibrium equation in the absence of body forces:

$$\dot{n}_{ij,i}(\mathbf{x}) = 0, \quad \mathbf{x} \in V_t; \tag{2.2}$$

boundary conditions

$$v_i(\mathbf{x}) = G_{ij}(\mathbf{x}) x_j, \quad \mathbf{x} \in S_t \tag{2.3}$$

and constitutive relation (2.1).

Applying the Green tensor technique, the solution of this problem may be presented in the form of the integral equation

$$g_{ij}(\mathbf{x}) = g^0_{ij}(\mathbf{x}) + \int_{V_t} \Gamma_{ijkl}(\mathbf{x}-\mathbf{x}')\, \delta l_{klmn}(\mathbf{x}') g_{nm}(\mathbf{x}')\, dV', \tag{2.4}$$

where g^0_{ij} is the solution of the homogeneous equivalent problem, $\Gamma_{ijkl}(\mathbf{x}-\mathbf{x}') = \mathcal{G}_{il,kj}(\mathbf{x}-\mathbf{x}')$, $\mathcal{G}_{ij}$ is the Green tensor, V_t presents the current volume of the material, S_t is its current external surface.

In order to obtain this expression, the tensor of the local properties of material has been decomposed on a constant part $\mathbf{L}^0$ and the deviation $\delta\mathbf{l}$ such that

$$l_{ijkl}(\mathbf{x}) = L^0_{ijkl} + \delta l_{ijkl}(\mathbf{x}). \tag{2.5}$$

Moreover, the $\mathbf{L}^0$ tensor is chosen to be symmetric with respect to second and fourth indices.

2.1. Formal solution of the integral equation

The formal solution of the integral equation (2.4) may be presented in a form of the development on multiple integrals. The approximation of zero order is obtained neglecting the integral term in Eq. (2.4). This leads to the so-called Taylor–Lin model

$$g_{ij}(\mathbf{x}) = g^0_{ij}(\mathbf{x}) = G_{ij}(\mathbf{x}). \tag{2.6}$$

The approximation of first order is accomplished by substituting $g_{ij}(\mathbf{x})$ in Eq. (2.4) by $g^0_{ij}(\mathbf{x})$. In this case one may write

$$g_{ij}(\mathbf{x}) = g^0_{ij}(\mathbf{x}) + \int_{V_t} \Gamma_{ijkl}(\mathbf{x}-\mathbf{x}')\, \delta l_{klmn}(\mathbf{x}') g^0_{nm}(\mathbf{x}')\, dV'. \tag{2.7}$$

Finally, substituting $g_{ij}(\mathbf{x})$ under integrals successively by new and more and more precise approximations, one has

$$(2.8)\qquad g_{ij}(\mathbf{x}) = g^0_{ij} + \int_{V'_t} \Gamma_{ijkl}(\mathbf{x}-\mathbf{x}')\,\delta l_{lkmn}(\mathbf{x}')\,g_{nm}(\mathbf{x}')\,dV' + \int_{V'} \int_{V'_t} + \Gamma_{ijlk}(\mathbf{x}-\mathbf{x}')\,\delta l_{klmn}(\mathbf{x}')\,\Gamma_{nmpq}(\mathbf{x}'-\mathbf{x}'')\,\delta l_{qprs}(\mathbf{x}'')\,g^0_{sr}(\mathbf{x}'')\,dV|dV'' + \ldots.$$

Expression (2.8) may be rewritten after factorizing g^0 in the form

$$(2.9)\qquad \mathbf{g}(\mathbf{x}) = \Big(\mathbf{I} + \int_{V'_t} \boldsymbol{\Gamma}(\mathbf{x}-\mathbf{x}'):\boldsymbol{\delta l}(\mathbf{x}')\,dV' + \int_{V'_t}\int_{V''_t} \boldsymbol{\Gamma}(\mathbf{x}-\mathbf{x}'): \boldsymbol{\delta l}(\mathbf{x}'):\boldsymbol{\Gamma}(\mathbf{x}'-\mathbf{x}''):\boldsymbol{\delta l}(\mathbf{x}'')\,dV'dV'' + \ldots\Big):\mathbf{g}_0(\mathbf{x})$$

or

$$(2.10)\qquad \mathbf{g}(\mathbf{x}) = \mathbf{a}(\mathbf{x}):\mathbf{g}_0,$$

where the $\mathbf{a}(\mathbf{x})$ operator is defined by the relation (2.9). One deduces the overall velocity gradient $\mathbf{G}$ from the expression (2.10) by averaging operation over the whole material volume

$$(2.11)\qquad \mathbf{G} = \frac{1}{V_t}\int_{V_t} \mathbf{g}(\mathbf{x})\,dV = \left(\frac{1}{V_t}\int_{V_t} \mathbf{a}(\mathbf{x})\,dV_t\right):\mathbf{g}^0 = \mathbf{A}:\mathbf{g}^0.$$

Expressions (2.10) and (2.11) lead finally to the concentration equation

$$(2.12)\qquad \mathbf{g}(\mathbf{x}) = \mathbf{a}(\mathbf{x}):\mathbf{A}^{-1}:\mathbf{G} = \mathbf{B}(\mathbf{x}):\mathbf{G}.$$

The overall properties of the polycrystal may now be found using the concentration equation. Indeed, introducing Eq. (2.12) into the relation (2.1), one has

$$\dot{\mathbf{n}}(\mathbf{x}) = \mathbf{l}(\mathbf{x}):\mathbf{B}(\mathbf{x}):\mathbf{G}$$

which, after averaging over all material volume, becomes

$$(2.13)\qquad \dot{\mathbf{N}} = \left(\frac{1}{V_t}\int_{V_t} \mathbf{l}(\mathbf{x}):\mathbf{B}(\mathbf{x})\,dV_t\right)\mathbf{G} := \mathbf{L}^{\mathrm{eff}}:\mathbf{G}.$$

Equations (2.12) and (2.13) remain valid irrespectively of the current internal structure of the inhomogeneous material.

2.2. One-site "quasi"-self-consistent method

In the case of the small elastoplastic strain theory, the one-site self-consistent method is obtained choosing the tangent properties of the reference medium to be equal to the effective ones and considering only the interactions between a given grain and the matrix characterized by $\mathbf{L}^{\mathrm{eff}}$. When the large elastoplastic deformations are considered, a similar approach is not possible because the tensor of the effective properties of the medium does not possess the symmetries required by $\mathbf{L}^0$. Accordingly, we propose to choose for $\mathbf{L}^0$ the symmetric part of $\mathbf{L}^{\mathrm{eff}}$

$$(2.14)\qquad L^0_{ijkl} = \frac{1}{2}\left(L^{\mathrm{eff}}_{ijkl} + L^{\mathrm{eff}}_{ilkj}\right).$$

In what follows we limit our consideration to the polycrystalline medium composed on grains of various crystallographic orientations (eventually various crystallographic structure). Supposing the uniform elastoplastic properties within each grain, the deviation part of the instantaneous moduli tensor may now be written as

$$\delta l_{ijkl}(\mathbf{x}) = \sum_{\mathrm{I}} \Delta l^{\mathrm{I}}_{ijkl}\,\theta^{\mathrm{I}}(\mathbf{x}), \tag{2.15}$$

where

$$\theta^{\mathrm{I}}(\mathbf{x}) = \begin{cases} 0 & \text{if} \quad \mathbf{x} \notin V_{\mathrm{I}}, \\ 1 & \text{if} \quad \mathbf{x} \in V_{\mathrm{I}} \end{cases}$$

and V_{I} is the volume of grain I.

Similarly, noting the average value of the velocity gradient over a grain I as

$$\mathbf{g}^{\mathrm{I}} = \frac{1}{V_{\mathrm{I}}} \int_{V_{\mathrm{I}}} \mathbf{g}(\mathbf{x})\,dV,$$

the field of the velocity gradient may be expressed:

$$\mathbf{g}(\mathbf{x}) = \sum_{\mathrm{I}} \mathbf{g}^{\mathrm{I}}\theta^{\mathrm{I}}(\mathbf{x}).$$

In consequence, the integral equation, after some simple algebra, becomes (see deta il in [9])

$$\mathbf{g}^{\mathrm{I}} = \mathbf{g}^{0} + \mathbf{T}^{\mathrm{II}} : \Delta\mathbf{I}^{\mathrm{I}} : \mathbf{g}^{\mathrm{I}}, \tag{2.16}$$

where

$$\mathbf{T}^{\mathrm{II}} = \frac{1}{V_{\mathrm{I}}} \int_{V_{\mathrm{I}}} \int_{V_{\mathrm{I}}} \boldsymbol{\Gamma}(\mathbf{x}-\mathbf{x}')\,dV_{\mathrm{I}}'\,dV_{\mathrm{I}}.$$

In this case

$$\mathbf{a}^{\mathrm{I}} = (\mathbf{I} - \mathbf{T}^{\mathrm{II}} : \Delta\mathbf{I}^{\mathrm{I}})^{-1},$$

$$\mathbf{A} = \sum_{\mathrm{I}} f^{\mathrm{I}}(\mathbf{I} - \mathbf{T}^{\mathrm{II}} : \Delta\mathbf{I}^{\mathrm{I}})^{-1},$$

$$\mathbf{B}^{\mathrm{I}} = (\mathbf{I} - \mathbf{T}^{\mathrm{II}} : \Delta\mathbf{I}^{\mathrm{I}})^{-1} : \Big[\sum_{\mathrm{I}} f^{\mathrm{I}}(\mathbf{I} - \mathbf{T}^{\mathrm{II}} : \Delta\mathbf{I}^{\mathrm{I}})^{-1}\Big]^{-1}$$

and

$$\mathbf{L}^{\mathrm{eff}} = \sum_{\mathrm{I}} f^{\mathrm{I}}\mathbf{I}^{\mathrm{I}} : \mathbf{B}^{\mathrm{I}}, \tag{2.17}$$

where f^{I} is the volume fraction of grains family with label I.

In the next sections we present the evolution laws for four microparameters describing the internal structure of the polycrystal as a function of the local velocity gradient.

3. Single crystal behavior. Evolution of critical shear stresses

The single crystal elastoplastic behavior at large strain has been developed by MANDEL [14], HILL and RICE [15], ASARO [16], NEMAT-NASSER [17] and is based on the additive decomposition of the strain rate into elastic and plastic parts.

$$g_{ij} = (d^e_{ij} + d^p_{ij}) + (w^e_{ij} + w^p_{ij}) \tag{3.1}$$

where the strain rate **d** and the spin **w** have been introduced.

The plastic part of **g** is supposed to result from the plastic slip on different glide systems defined by the normal vectors to the glide plane **n** and the slip direction vectors **m**. Thus

$$g^p_{ij} = \sum_h m^h_i n^h_j \dot{\gamma}^h, \tag{3.2}$$

where $\dot{\gamma}^h$ is the plastic slip rate on system h.

Decomposing the expression (3.2) into symmetric and antisymmetric parts, one has

$$d^p_{ij} = \frac{1}{2} \sum_h (m^h_i n^h_j + m^h_j n^h_i) \dot{\gamma}^h = \sum_h R^h_{ij} \dot{\gamma}, \tag{3.3}$$

$$w^p_{ij} = \frac{1}{2} \sum_h (m^h_i n^h_j - m^h_j n^h_i) \dot{\gamma}^h = \sum_h Q^h_{ij} \dot{\gamma}^h. \tag{3.4}$$

The elastic constitutive relation is supposed to be

$$\overset{\nabla}{\sigma}{}^*_{ij} = C_{ijkl} d^e_{lk} - \sigma_{ij} d^e_{kk}, \tag{3.5}$$

where C_{ijkl} is the matrix of the elasticity constants and

$$\overset{\nabla}{\sigma}{}^*_{ij} = \dot{\sigma}_{ij} - w^e_{ik}\sigma_{kj} + \sigma_{ik} w^e_{kj} \tag{3.6}$$

is the Jaumann–Zaremba true stress rate with respect to the crystal lattice. The relation between nominal stress rate $\dot{n}_{ij}$ and $\dot{\sigma}_{ij}$

$$\dot{n}_{ij} = \dot{\sigma}_{ij} - (d_{ik} + w_{ik})\sigma_{kj} + \sigma_{ij} d^e_{kk} \tag{3.7}$$

leads to

$$\dot{n}_{ij} = C_{ijkl} d_{kl} - d_{ik}\sigma_{kj} - \sigma_{ki} w_{kj} - \sum_g (C_{ijkl} R^g_{kl} + Q^g_{ik}\sigma_{kj} - Q^g_{kj}\sigma_{ik}) \dot{\gamma}^g. \tag{3.8}$$

The above expression determines the behavior of the single crystal. In order to eliminate the unknown $\dot{\gamma}^g$ in this relation, one has to establish, as it is common in plasticity: the yield criterion, flow rule and evolution law for the yield stress of the single crystal. When classical plasticity of the single crystal is considered, the Schmid law corresponds to the yield criterion. It states that the plastic glide may take place on the g-th slip system if the resolved shear stress on this system reaches some critical value noted τ_c

$$f^g(\sigma_{ij}, \gamma_1, \gamma_2, \ldots, \gamma) = R^g_{ij}\sigma_{ij} - \tau^g_c(\gamma_1, \gamma_2, \ldots, \gamma_u) = 0. \tag{3.9}$$

It is obvious that the relation (3.3) in such a situation defines the corresponding flow rule.

The linearized law for the critical shear stress evolution has been proposed by MANDEL [14] and may be written in the form

$$\dot{\tau}_c^g = \sum_h H^{gh} \dot{\gamma}^h, \tag{3.10}$$

where summation is performed on all active systems and H^{gh} is the so-called microscopic hardening matrix.

The experimental results on copper and aluminium single crystals [18, 19] indicate a very complicated dependence among all the slip systems for different primary shear strain in stage I. Nevertheless, the hardening matrix may be supposed to be constant, at least for stage II, and composed in four terms reflecting short range interactions between primary and latent dislocations [18]:

H0 is the self hardening term,

H1 is the term describing interactions between dislocations on coplanar or colinear systems,

H2 defines the systems leading to formation of glissile junctions,

H3 describes Lomer–Cottrell sessile locks formation

and such that H0 < H1 < H2 < H3.

Still, according to, [18] the hardening matrix for FCC single crystals may be presented in the form

$(H^{hg}) =$

A2	A3	A6	B2	B4	B5	C1	C3	C5	D1	D4	D6	
H0	H1	H1	H1	H2	H2	H1	H2	H3	H1	H3	H2	A2
H1	H0	H1	H2	H1	H3	H2	H1	H2	H3	H1	H2	A3
H1	H1	H0	H2	H3	H1	H3	H2	H1	H2	H2	H1	A6
H1	H2	H2	H0	H1	H1	H1	H3	H2	H1	H2	H3	B2
H2	H1	H3	H1	H0	H1	H3	H1	H2	H2	H1	H2	B4
H2	H3	H1	H1	H1	H0	H2	H2	H1	H3	H2	H1	B5
H1	H2	H3	H1	H3	H2	H0	H1	H1	H1	H2	H2	C1
H2	H1	H2	H3	H1	H2	H1	H0	H1	H2	H1	H3	C3
H3	H2	H1	H2	H2	H1	H1	H1	H0	H2	H3	H1	C5
H1	H3	H2	H1	H2	H3	H1	H2	H2	H0	H1	H1	D1
H3	H1	H2	H2	H1	H2	H2	H1	H3	H1	H0	H1	D4
H2	H2	H1	H3	H2	H1	H2	H3	H1	H1	H1	H0	D6

where the letters A, B, C, D indicate four planes $(\bar{1}\,1\,1)$, $(1\,1\,1)$, $(\bar{1}\,\bar{1}\,1)$, $(1\,1\,1)$ and numbers 1, 2, 3, 4, 5 and 6 the slip directions $\langle 0\,1\,1\rangle$, $\langle 0\,\bar{1}\,1\rangle$, $\langle 1\,0\,1\rangle$, $\langle \bar{1}\,0\,1\rangle$, $\langle \bar{1}\,1\,0\rangle$, $\langle 1\,1\,0\rangle$, respectively.

It is obvious that this constant hardening matrix constitutes only the first-order approximation of the real phenomenon of interaction, creation and annihilation of dislocations during any plastic deformation of the single crystal. Nevertheless, this rather rough descrip

tion induces realistic responses when modelling the polycrystal behavior, as it can be discovered in the following sections.

As in the case of phenomenological plasticity, the given slip system becomes really active if and only if the stress vector remains on the yield surface. This condition can be written in the following form:

$$\dot{f}^g = \dot{\widehat{R^g_{ij}\sigma_{ij}}} - \dot{\tau}^g_c = 0$$

or, after some algebra,

$$R^g_{ij}\overset{\nabla}{\sigma}{}^*_{ij} = \sum_h H^{gh}\dot{\gamma}^h. \tag{3.11}$$

Now, combining the above equations, one can deduce the expression for $\dot{\gamma}^g$

$$\dot{\gamma}^g = \sum_h M^{gh}(R^h_{ij}C_{ijkl}d_{kl} - R^h_{ij}\sigma_{ij}d_{kk}), \tag{3.12}$$

where

$$M^{gh} = (H^{gh} + R^h_{ij}C_{ijkl}R^h_{kl})^{-1}.$$

Introducing Eq. (3.12) into Eq. (3.8), the final expression for the single crystal behavior is obtained:

$$\dot{n}_{ij} = \left[C_{ijkl} - \frac{1}{2}(\delta_{ik}\sigma_{ij} + \delta_{il}\sigma_{kj}) + \frac{1}{2}(\delta_{jl}\sigma_{ki} - \delta_{jk}\sigma_{li}) - \sum_{g,h}(C_{ijmn}R^g_{mn} + Q^g_{im}\sigma_{mj} - Q^g_{mj}\sigma_{mi})M^{gh}(R^h_{pq}C_{pqkl} - R^h_{pq}\sigma_{pq}\delta_{kl})\right] g_{lk},$$

which has the form of Eq. (2.1).

In order to model the polycrystal behavior, one has to follow the evolution of the critical shear stress on each slip system and for all grains of the aggregate.

In the next chapter we discuss the evolution laws for the morphological and crystallographic textures as well as for the internal stresses.

4. Morphological and crystallographic textures. Internal stresses

In this chapter we discuss the evolution laws for the three remaining internal structure parameters and their influence on the macroscopic behavior of a polycrystal. This discussion is supported by a few examples of numerical calculations performed for the FCC polycrystal represented by 100 ellipsoidal inclusions whose initial crystallographic orientations are random. The elasticity of the individual grain as well as that of the polycrystal is supposed to be isotropic and defined by two Lamé's constants. The initial value of the critical shear stress for all slip systems is chosen to be the same. It is assumed that the hardening matrix may be defined by only two different terms such that H_w = H0 = H1 which represents weak interactions whereas H_F = H2 = H3 describes strong ones. All calculations have been performed for $H_w = \mu/250$ and various values of the anisotropy parameter $A = H_F/H_w$. The value of $H_w = \mu/250$ corresponds to stage II of the single crystal behavior.

4.1. Evolution of grain shape and principal axes orientation

In what follows we assume to know the velocity gradient g^I for all inclusions.

$$\mathbf{g}^I = \mathbf{B}^I : \mathbf{G}. \tag{4.1}$$

The decomposition of $\mathbf{g}^I$ on the strain rate tensor $\mathbf{d}$ and spin $\mathbf{w}$ enables us to determine the stretching of the principal axes (fibers) of the I-th inclusion as well as their rotations. Indeed, it is easy to show that

$$\begin{aligned} \partial_\tau \mathbf{U}_{|\tau=t} &= \mathbf{d}, \\ \partial_\tau \mathbf{R}_{|\tau=t} &= \mathbf{w}, \end{aligned} \tag{4.2}$$

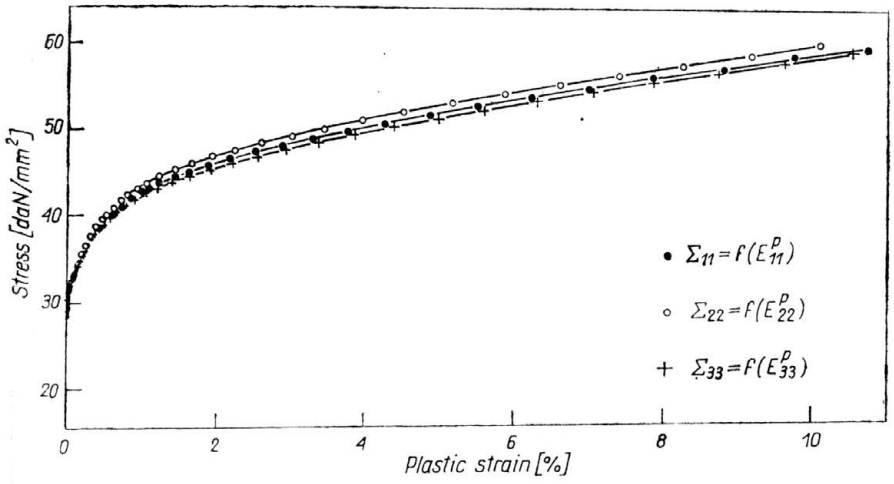

FIG. 1. Tensile curves at three orthogonal directions showing the initial isotropy of the polycrystal.

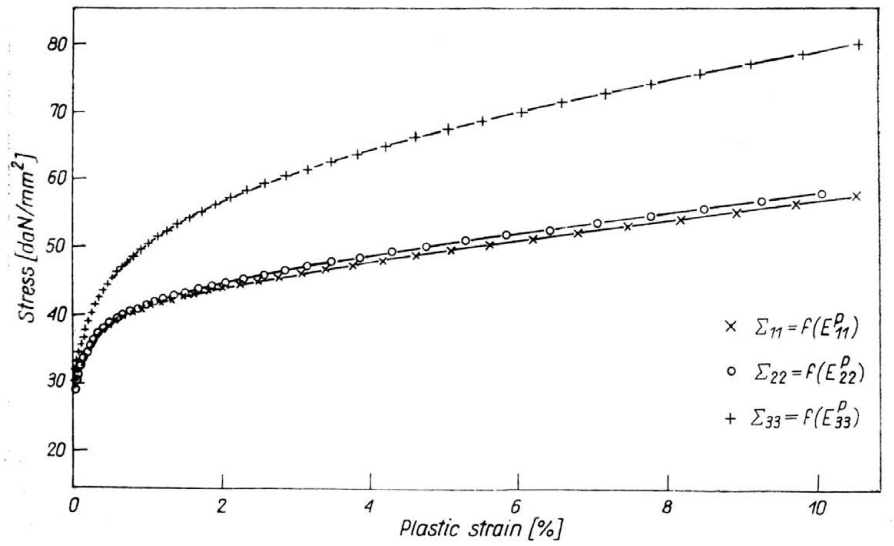

FIG. 2. Influence of the initial morphological texture on the anisotropy of the tensile curves. The grain aspect ratio is defined by $a/c = b/c = 5$.

the rate of stretch and rotation tensors with respect to the current configuration, are equal to the strain rate and spin tensors. The mapping **U** stretches the principal fibers without change of angles between them as it is known from the polar decomposition. From the above we conclude that the evolution of the morphological texture is imposed by the velocity gradient $\mathbf{g}^{\mathrm{I}}$.

In order to show the influence of the morphological texture on the overall behavior of a polycrystal, different initial grain shapes have been chosen. The amplitude of the plastic strain has been limited to about 10%. For such a strain it can be assumed that the induced morphological and crystallographic textures are negligible. Figure 1 presents three tensile curves in Σ_{11}, Σ_{22}, and Σ_{33} directions when a spherical shape of inclusions has been chosen. This figure indicates a good isotropic behavior of the modelled polycrystal. The influence of the initial morphological texture on the anisotropy of the aggregate is illustrated in Fig. 2. Once more, three tensile curves in three orthogonal directions are plotted in this figure but this time for disk-shaped inclusions with the principal axes parallel to the reference frame and such that $a/c = b/c = 5$. A very pronounced anisotropic behavior is visible. As it could be expected, the two tensile curves in Σ_{11} and Σ_{22} directions are still very similar but their level is lower than in the case of spherical inclusions. Σ_{33}, as the function of E^p_{33} curve, is in turn much higher. For example, the difference between the flow stresses at $E^p \simeq 10\%$ in Σ_{33} and Σ_{11} directions is about 40% with respect to the Σ_{11} value. Figures 3 and 4 illustrate the anisotropy of the overall behavior of the polycrystal

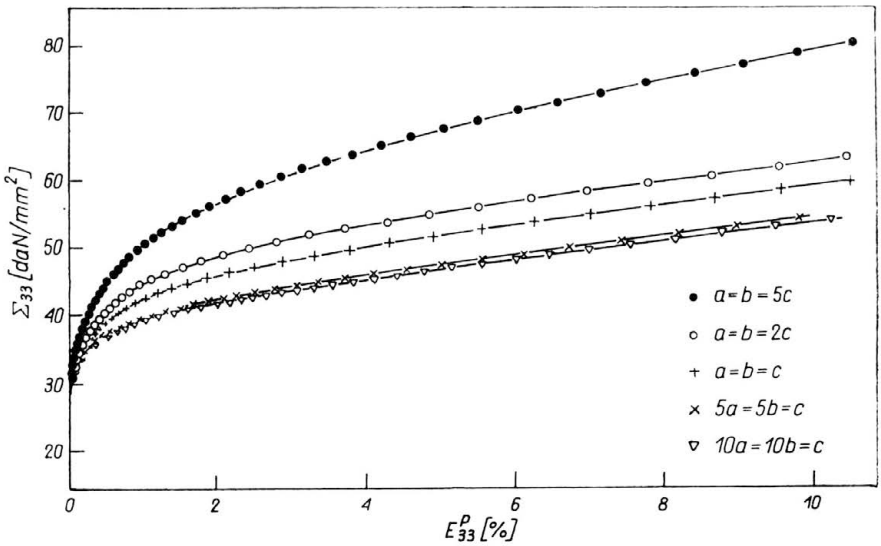

FIG. 3. Tensile curves $\Sigma_{33} = f(E^p_{33})$ for various grain aspect ratios $a/c = b/c = 5, 2, 1, 0.2, 0.1$.

for five various inclusion aspect ratios. The circular shape of grain has been assumed in 1–2 plane and the third principal axis has been changed from $a/c = 5$ to $a/c = 0.1$. Figure 3 shows the corresponding tensile curves in the 3-direction. The presented results illustrate the importance of the grain shape on the constitutive relation. Figure 4 indicates the anisotropy in the 1-(or 2)-direction. The effect of the grain shape is less important but still

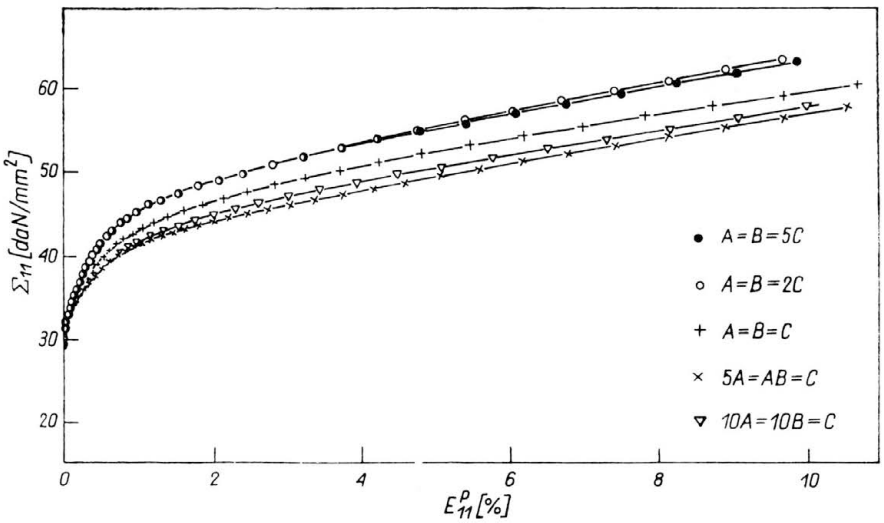

FIG. 4. Tensile curves $\Sigma_{11} = f(E^p_{11})$ for various grain aspect ratios $a/c = b/c = 5, 2, 1, 0.2, 0.1$.

remains of the first order. It should be emphasized that the curve sequences in these two figures are inverted.

It is straightforward to conclude the influence of the morphology of the grain on initial (and subsequent) yield surfaces. This aspect of the morphological texture was discussed by the authors in [20].

4.2. Induced crystallographic texture

Crystallographic texture development is characterized by a nonuniform evolution of the lattice spin field **w***, which can be calculated as the elastic part of the total spin, which in turn is obtained from the relation (4.1) by the antisymmetrization operation.

$$\mathbf{w}^{e^{\mathrm{I}}} = \frac{1}{2}[\mathbf{B}^{\mathrm{I}}:\mathbf{G} - (\mathbf{B}^{\mathrm{I}}:\mathbf{G})^T] - \mathbf{w}^{p^{\mathrm{I}}}, \tag{4.3}$$

where $\mathbf{w}^{p^{\mathrm{I}}}$ is given by the expression (3.4). Knowing the concentration tensor $\mathbf{B}^{\mathrm{I}}$ and plastic slip amplitudes $\dot{\gamma}^h$ of all active systems for the given grain I, it is possible to determine $\mathbf{w}^{e}$.

Usually, the crystallographic orientation of grains is determined by three Euler angles, say φ_1, Φ, φ_2, measured with respect to some fixed coordinate system. The rate of change of the Euler angles may be related with the elastic spin $\mathbf{w}^{e^{\mathrm{I}}}$ as follows [21]:

$$\dot{\varphi}_1^{\mathrm{I}} = \frac{\sin\varphi_2}{\sin\Phi} w_{13}^{e^{\mathrm{I}}} - \frac{\cos\varphi_2}{\sin\Phi} w_{23}^{e^{\mathrm{I}}},$$

$$\dot{\Phi}^{\mathrm{I}} = -\cos\varphi_2 w_{23}^{e^{\mathrm{I}}} + \sin\varphi_2 w_{13}^{e^{\mathrm{I}}},$$

$$\dot{\varphi}_2^{\mathrm{I}} = \cos\Phi\left[\frac{\cos\varphi_1}{\sin\Phi} w_{13}^{e^{\mathrm{I}}} + \frac{\sin\varphi_1}{\sin\Phi} w_{23}^{e^{\mathrm{I}}}\right] + w_{21}^{e^{\mathrm{I}}}.$$

In this study we follow the orientation of all grains as a function of the Eulerian plastic strain and illustrate the texture evolution by the inverse pole figures. The tensile and compression test simulations are presented in this paper. Figure 5a exhibits the initial texture of the polycrystal which may be supposed to be isotropic. Figures 5b and 5c illustrate the induced textures for 31% and 102% of plastic strain during the tensile test. The double

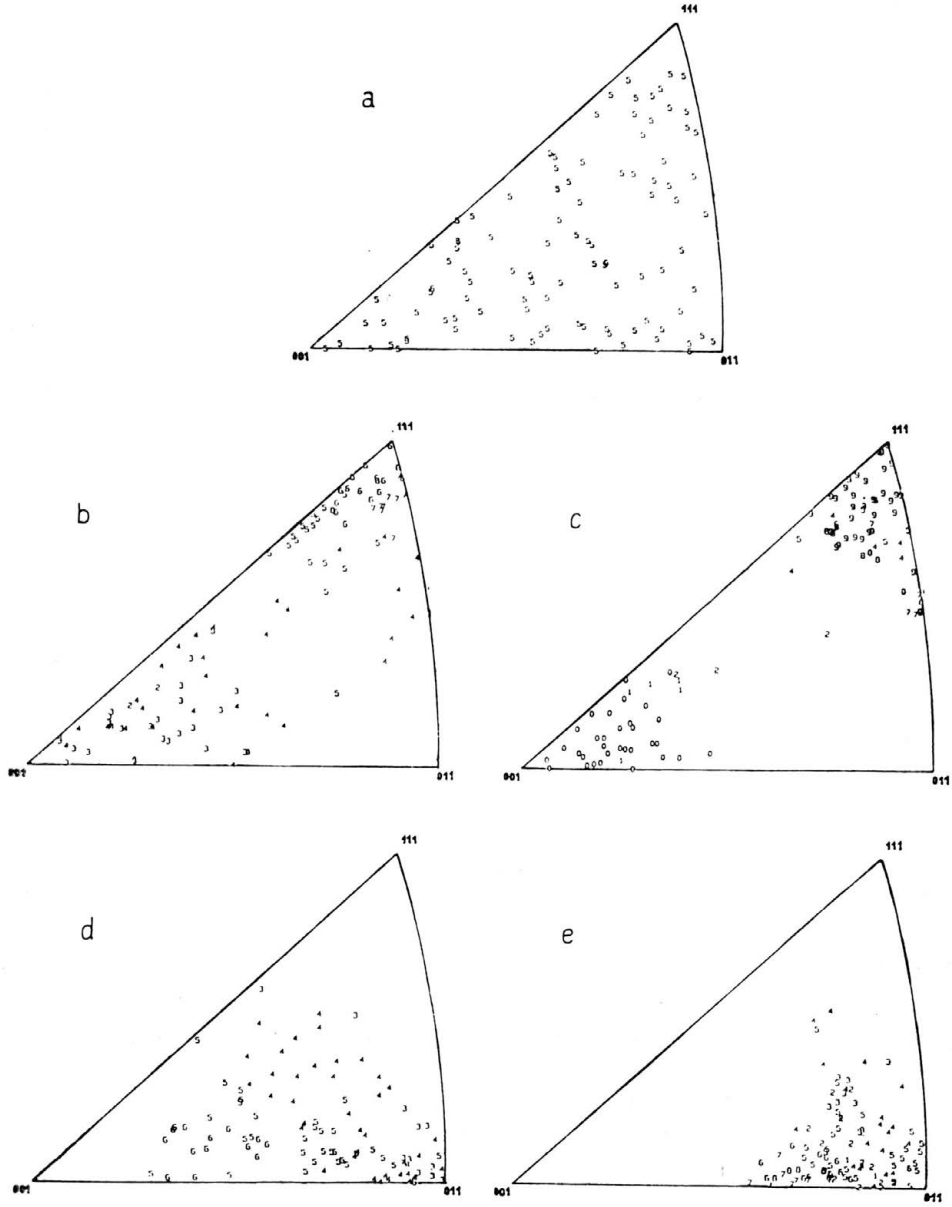

FIG. 5. Induced crystallographic texture and internal stresses; a) initial texture, b) and c) tensile test, d) and e) compression test.

texture of $\langle 1\ 1\ 1\rangle$ and $\langle 1\ 0\ 0\rangle$ fiber axes is obtained with good agreement with experimental results for FCC polycrystals.

In the case of the compression test simulation, the same initial texture of Fig. 5a has been used. Figures 5d and 5e present the development of the $\langle 1\ 1\ 0\rangle$ texture for 31% and 71% of the plastic strain. Once again the obtained results conform with the experimental observations [22]. The numbers used to refer the orientation of the tensile axis with respect to the crystal axes $\langle 1\ 1\ 1\rangle$, $\langle 1\ 0\ 0\rangle$ and $\langle 1\ 1\ 0\rangle$ indicate also the level of the σ_{33}-component of the internal (residual) stress tensor for each family of grains, the third axis being the tensile or compression direction. The levels of internal stresses are given by the Table 1.

Table 1.

Stress level	Stress limits	
	Lower	Upper
0	−50	−40
1	−40	−30
2	−30	−20
3	−20	−10
4	−10	0
5	0	10
6	10	20
7	20	30
8	30	40
9	40	50

These indications are discussed in details in the following section concerning the evolution of second-order internal stresses for elastoplastic polycrystals.

4.3. Second order internal stresses

The relative misorientation of the grains of the polycrystal and the plastic anisotropy of the single crystal generate, during plastic straining of the material, internal stresses of second order, i.e. the stresses at the grain level. These stresses play an important role in the hardening phenomenon which is well manifested during complex path loadings. On the other hand they contribute to an increase of the stored energy of the material [23].

The model presented in this study enables us to calculate the residual stresses inside each grain and to follow their evolution in the function of the plastic strain.

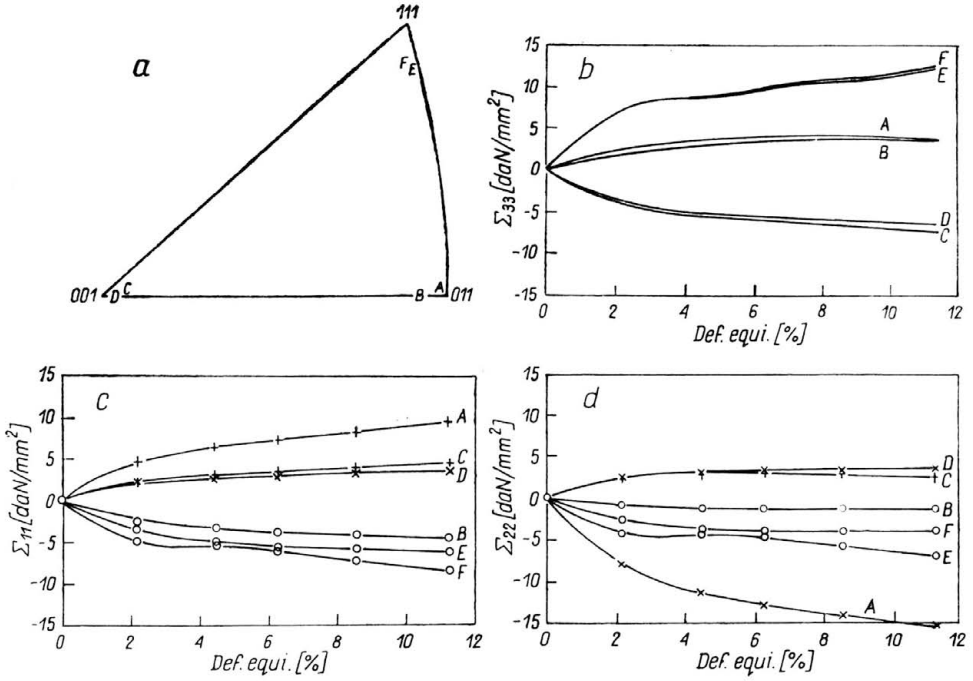

FIG. 6. Internal stress evolution for six different grains of various crystallographic orientations shown in Figure a. Figures b, c and d illustrate the evolutions of Σ_{33}, Σ_{11}, and Σ_{22} components, respectively.

Figure 6 depicts the evolution of the internal stresses for six particular grains denoted by A, B, C, D, E and F whose initial orientations are shown in Fig. 6a. The components σ_{33}, σ_{11}, and σ_{22} are plotted in Figs. 6b, 6c and 6d, respectively, as a function of the E_{33} component of the plastic strain tensor.

The internal stresses become negative or positive according to the orientation of grains. Their evolution is fast during the first stage of deformation and next the stabilization tendency is visible referring to Fig. 6. The level of the internal stresses is far from being

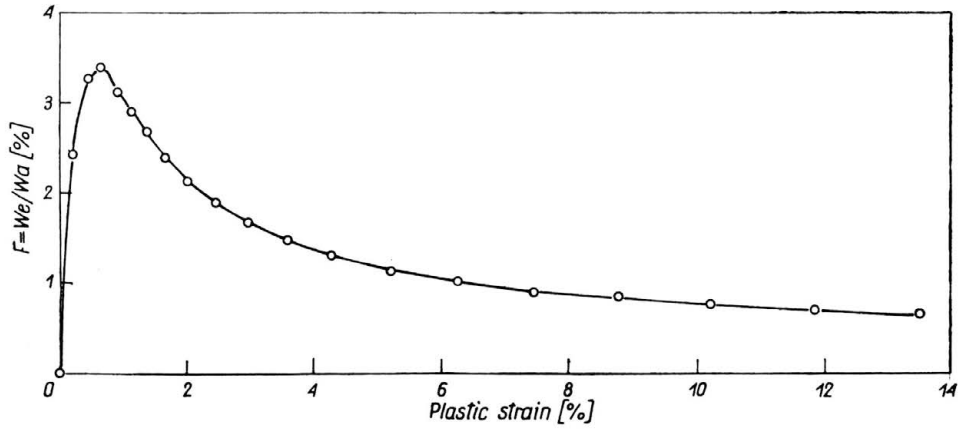

FIG. 7. Evolution of the stored energy fraction $f = We/Wa$ versus plastic strain.

negligible. For instance, for the plastic strain of about 5% the contribution of internal stresses is about 10% to 30% of the applied stresses as it can be concluded from Figs. 1 and 6. They contribute in a significant manner to the stored energy of the material. Figure 7 shows the evolution of the fraction of the stored energy We/Wa as a function of the plastic strain imposed on the polycrystal. We is the stored energy associated with the second-order internal stresses and Wa is the anelastic energy furnished during the deformation process whose part Q is dissipated in the form of heat and another part is stored in the material.

The influence of the crystallographic orientation of grains on the second order internal stresses is depicted in Fig. 5. Figures 5b and 5c (tensile test) show that the grains whose final orientation tends to approach the $\langle 1\ 1\ 1\rangle$ axis are characterized by a positive residual stress σ_{33} and the grains which tends towards the $\langle 100\rangle$ final orientation are in compression. By definition the system of internal stresses is self-equilibrated, this means

$$\int_{V_t} \sigma_{ij}(\mathbf{x})\, dV = 0,$$

which is of course verified in this case.

The difference between the grains of $\langle 1\ 1\ 1\rangle$ and $\langle 1\ 0\ 0\rangle$ types results from a different hardening. It is well documented [24] that a single crystal of $\langle 1\ 1\ 1\rangle$ orientation exhibits more important hardening than that from a vicinity of the $\langle 1\ 0\ 0\rangle$ orientation. This different behavior explains the sign of the residual stresses presented in Figs. 5b and 5c.

The results concerning the simulation of a compression test are more difficult to analyze because the stable orientation in this case is unique and close to (110); nevertheless one can conclude from Fig. 5e that the system of the internal stresses is self-equilibrated in such a manner that grains in compression are localized on the (110)–(112) lines and surrounded by grains in tension.

Conclusions

A very complete model for elastoplastic behavior of the polycrystal is proposed in this study which is based on the physical fields describing the internal structure of the material. These microparameters are generally accessible by experiment. This self-consistent model constitutes a particular approximation of the exact integral equation derived for the finite elastoplastic strains. The model has been used in order to simulate the influence of the initial morphological texture, induced crystallographic texture, and internal stress development on the macroscopic behavior of the polycrystal. All numerical results obtained by these simulations coincide very well with the experimental data. The fundamental phenomenon concerning the stored energy evolution with the plastic strain has been demonstrated. It must be emphasized that all phenomenological approaches predict the continuously increasing function of the fraction of the stored energy during the deformation process. It is in contradiction with the experimental results [25, 26].

References

1. E. KRÖNER, *Graded and perfect disorder in random medium elasticity*, J. Eng. Mech. Div., ASCE, 106, 889–914, 1980.

2. P. H. DEDERICHS and R. ZELLER, *Variational treatment of the elastic constants of disordered materials*, Z. Physik, 259, 103–116, 1973.
3. E. KRÖNER, *Linear properties of random media: The systematic theory*, in: Cahiers du Groupe Française de Rhéologie, 15éme Colloque Annuel du Groupe Francaise de Rhéologie, Paris, 15–40, 1980.
4. G. SACHS, *Zur Ableitung einer Fliessbedingung*, Z. der V.D.I. **72**, 739–748, 1928.
5. G. I. TAYLOR, *The mechanism of plastic deformation of crystals*, Proc. Roy. Soc. London A 145, 362–387, 1934.
6. J. W. HUTCHINSON, *Elastic-plastic behaviour of polycrystalline metals and composites*, Proc. Roy. Soc London A139, 247–272, 1970.
7. M. BERVEILLER and A. ZAOUI, *An extension of the self-consistent scheme to plastically flowing polycrystals*, J. Mech. Phys. Sol, 26, 325–344, 1979.
8. A. HIHI, M. BERVEILLER and A. ZAOUI, *Une nouvelle formulation de la modélisation autocohérente de la plasticité des polycristaux métalliques*, J. Mec. Théorique et Appliquée, 4, 201–221, 1985.
9. P. LIPINSKI and M. BERVEILLER, *Elastoplasticity of micro-inhomogeneous metals at large strains* [to appear in Int. J. of Plasticity].
10. R. J. ASARO, *Micromechanics of crystals and polycrystals*, Adv. in Appl. Mech. **23**, 1–115, 1983.
11. S. AHZI, G. CANOVA, A. MOLINARI, *A self-consistent approach of the large deformation polycrystal viscoplasticity*, [to appear in Acta Met.].
12. T. IWAKUMA, S. NEMAT-NASSER, *Finite elastic plastic deformation of polycrystalline metals and composites*, Proc. Roy. Soc., A394, 87–115, 1984.
13. R. HILL, *Continuum micro-mechanics of elastoplastic polycrystals*, J. Mech. Phys. Solids, **13**, 89–101, 1965.
14. J. MANDEL, *Sur la définition de la vitesse de déformation élastique et sa relation avec la vitesse de contrainte*, Int. J. Solids Structures, **17**, 873–878, 1981.
15. R. HILL, J. R. RICE, *Constitutive analysis of elastic-plastic crystals at arbitrary strain*, J. Mech. Phys. Solids, **20**, 401–413, 1972.
16. R. J. ASARO, *Geometrical effects in the inhomogeneous deformation of ductile single crystals*, Acta Met. **27**, 445–453, 1979.
17. S. NEMAT-NASSER, *Decomposition of strain measures and their rates in finite deformation elastoplasticity*, Int. J. Solids Structures, **15**, 155–166, 1979.
18. P. FRANCIOSI, M. BERVEILLER, A. ZAOUI, *Latent hardening in copper and aluminium single crystals*, Acta Metall., **28**, 273–283, 1980.
19. P. FRANCIOSI, A. ZAOUI, *Multislip in F.C.C. Crystals a theoretical approach compared with experimental data*, Acta Metall., **30**, 1627–1637, 1980.
20. P. LIPINSKI, F. CORVASCE, M. BERVEILLER, *Effect of morphological texture on the overall elastoplastic behaviour of metallic polycrystals*, 8th Riso International Symp. Constitutive Relations and Their Physical Bases, 409–414, 1987.
21. H. J. BUNGE, *Some applications of the Taylor theory of polycrystal plasticity*, Kristall und Technik, 5, 145–175, 1970.
22. H. J. BUNGE, *Mathematische Methoden der Textur Analyse*, Akademie Verlag, Berlin 1969.
23. M. B. BEVER, D. L. HOLT, A. L. TITCHENER, *Stored energy in cold work*, Prog. Mat. Sci., **17**, 1–190, 1973.
24. B. JAOUL, *Etude de la plasticité et applications aux* métaux, Dunod ed., Paris, 1965.
25. A. CHRYSOCHOOS, *Bilan energétique en plasticité grandes déformations*, Rapport Greco n° 130/1984 et Thése I.D., Université Montpellier II, 1983.
26. F. CORVASCE, P. LIPINSKI, M. BERVEILLER, [to be published].

LABORATOIRE DE PHYSIQUE ET MECANIQUE DES MATERIAUX
NS TITUT SUPERIEUR DE GENIE MECANIQUE ET PRODUCTIQUE, METZ, FRANCE.

Received March 24, 1988.